Earth-Science Reviews 221 (2021) 103810

Contents lists available at ScienceDirect

Earth-Science Reviews

journal homepage: www.elsevier.com/locate/earscirev

(Paleo)oceanography of semi-enclosed seas with a focus on the Mediterranean region; Insights from basic theory

Paul Meijer *

Department of Earth Sciences, Utrecht University, PO Box 80.115, 3508 TC Utrecht, Netherlands

ARTICLE INFO

Keywords:
Paleoceanography
Semi-enclosed seas
Sea straits
Mediterranean sea
Messinian salinity crisis
Sapropels

ABSTRACT

To provide context for the interpretation of their sedimentary and paleoceanographic record, semi-enclosed seas are here investigated through the application of basic theory. The principles of conservation of water, salt and heat, in combination with a representation of flow through the seaway to the ocean, are used to chart how basin geometry, connectivity and atmospheric forcing together control basin-averaged salinity and temperature and the exchange flux. Data on present-day semi-enclosed seas of the wider Mediterranean region are used for illustration. First, ignoring the heat balance and with forcing constant in time, a dimensionless form of the governing equations is derived which clarifies the role of the various controlling parameters. This is applied to aspects of the Messinian Salinity Crisis. In the second part of the analysis the forcing is made a generalised periodic function of time. This informs us how basin salinity, its amplitude of variation and lag relative to the forcing, depend on basin and strait properties and varies with the period of forcing. Insights are applied to the precessional variation observed in the record of the Mediterranean Sea. In the third and fourth part of the analysis we include the balance of heat and basin-averaged temperature. Examination of the budget equations allows us to derive a relationship between the average air-sea heat flux and basin restriction. Finally, re-introducing strait flow, we study the interplay of basin temperature and salinity and establish under which conditions heat flux and temperature play a role, in addition to net evaporation and salinity.

1. Introduction

Semi-enclosed seas are basins that are land-locked apart from the presence of one or more seaways to the ocean or to an adjacent basin. This configuration arises early in the plate-tectonic development of an ocean, at rifting and incipient seafloor spreading (e.g. Red Sea, Gulf of California), as well as near the end of its life cycle, trapped between two converging continents (e.g. Mediterranean Sea). In the latter situation but also near the margins of a large ocean, semi-enclosed seas may further form by extension of the lithosphere overlying a subduction zone (back-arc spreading, e.g. Aegean Sea, Sea of Japan). Because the influence of the ocean is limited, the water properties and circulation of a semi-enclosed basin are sensitive to tectonic and climatic change. Tectonics may directly affect the ocean gateway and thus the state of restriction. It may also change the very shape of the basin. Climate change can exert its influence through sea-level induced changes in gateway depth, changes in the air-sea fluxes of water and heat and in variations in the amount of river water received from the adjacent continents. The semi-enclosed sea also feeds back to the climate system. The Nordic seas contributing dense waters to the Atlantic overturning circulation are essentially semi-enclosed basins. Dense outflow through the Strait of Gibraltar is an element of the same thermohaline system (Johnson et al., 2019). Moreover, the near land-locked seas may exert an influence on the climate of the adjacent land areas (Zhang et al., 2014).

The augmented sensitivity to tectonics and climate is expressed in the sedimentary record of the semi-enclosed basin in the form of pronounced cyclicity in terms of lithology, fossil content and chemistry (e.g. stable-isotope composition). Organic-rich deposits and, even, evaporites may be encountered in their sedimentary record. All of this holds true for the focus of this article, the basins of the wider Mediterranean region (Fig. 1). The rich sedimentary record of the Mediterranean proper, studied by drilling and accessible on land due to subsequent tectonic uplift, forms the basis for many detailed reconstructions of the geological history of the region. The cyclicity of its sediments, deciphered in terms of the various periodicities of Milankovitch variation in insolation, underlies the international time scale for the Neogene (Hilgen et al., 2012). Exploiting the link between gateway depth and the oxygen-isotope composition of carbonates, the record provides us with a

* Corresponding author.
E-mail address: p.meijer@uu.nl.

https://doi.org/10.1016/j.earscirev.2021.103810
Received 28 April 2021; Received in revised form 5 September 2021; Accepted 10 September 2021
Available online 11 September 2021

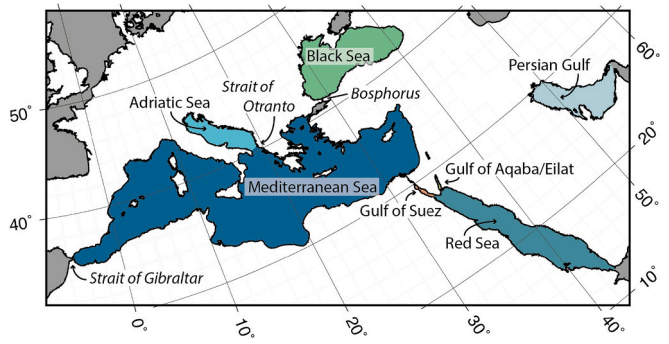

Fig. 1. Overview of semi-enclosed basins and sea straits discussed in paper. Oblique Mercator projection centred on southern Greece (base map created with GMT, Wessel et al., 2013). No relation between colours and basin properties intended.

history of global sea level for the last 5 Myr (Rohling et al., 2014).

It follows from the previous that it is pertinent, also from a geological point of view, to understand how exactly the properties and circulation of a semi-enclosed basin are controlled. This paper aims to make a contribution through the application of theory and modelling. We will explore and review what can be learned from the most basic representation of a semi-enclosed sea: a single reservoir connected to the ocean by a single seaway. The theory used will be limited to conservation laws for water, salt and heat, and a simplified representation of strait flow. For one, these form a robust toolbox with which to venture into the geological past. Focussing on the present-day state, Cessi et al. (2014) analysed the budget of several semi-enclosed seas in terms of energy.

The results of our analysis provide a physics-based context for the interpretation of sedimentary and paleoceanographic observations. Data on extant basins of the wider Mediterranean (Table 1 and Fig. 1) will be used to illustrate and exemplify. The paper is organised by the basic principles applied. Each starting point will prove to offer its own insight. Skipping the theoretical underpinning is possible, its aim is briefly explained at the start of each section and Table 2 explains the meaning of all variables and constants. Each block of theory is followed by one or two applications. In application 1 we examine the factors that control salinity and in particular look at how restriction of the oceanic connection affects salinity and time to equilibrium. In application 2 the case of the marginal basins of the Mediterranean Sea during the gypsum stage of the Messinian Salinity Crisis is investigated. Application 3 establishes the basics of the response of basin salinity to a periodic climatic forcing and in application 4 this is elaborated for the effect of precession on the Mediterranean sedimentary record. Considering the budget not only of water and salt but also of heat, application 5 examines the relation between restriction and the average heat flux between air and sea. In application 6 it is shown that, in general, temperature has a subordinate effect to salinity but this is nuanced in application 7 which focusses on basins that are prone to a switch in the sense of exchange (estuarine or anti-estuarine) at their strait.

Table 2
Explanation of all variables and constants used in text.

Symbol	Unit	Explanation
α	$^\circ C^{-1}$	Thermal expansion coefficient ($2 \times 10^{-4}\ ^\circ C^{-1}$)
β	–	Haline contraction coefficient (7.5×10^{-4})
γ	$m\ s^{-1}$	Relaxation coefficient
$\Delta S'$	–	Amplitude of variation of dimensionless salinity
$\Delta t'$	–	Lag of dimensionless time
ρ_b	$kg\ m^{-3}$	Density of basin water
ρ_o	$kg\ m^{-3}$	Density of ocean water
ρ_{ref}	$kg\ m^{-3}$	Reference density ($1029\ kg\ m^{-3}$)
τ	s	Characteristic time scale
A	m^2	Basin surface area
C_p	$J\ kg^{-1}\ ^\circ C^{-1}$	Specific heat of seawater ($3990\ J\ kg^{-1}\ ^\circ C^{-1}$)
c	$m^3\ s^{-1}$	Strait efficiency, units can also be $m^3\ s^{-1}\ (kg\ m^{-3})^{-1/2}$ or $m^3\ s^{-1}\ (kg\ m^{-3})^{-1}$
E	$m\ s^{-1}$	Rate of evaporation
e	$m\ s^{-1}$	Net rate of evaporation, $e = (E - P) - R/A$
e_a	$m\ s^{-1}$	Amplitude of net evaporation in case of periodic variation
e_m	$m\ s^{-1}$	Mean of net evaporation in case of periodic variation
H	$W\ m^{-2}$	Net air-sea heat flux
h	m	Average basin depth
P	$m\ s^{-1}$	Rate of precipitation
p	s	Period of variation of forcing
p'	–	Dimensionless period of variation of forcing
Q_b	$m^3\ s^{-1}$	Volume flux of water outflow from basin
Q_o	$m^3\ s^{-1}$	Volume flux of ocean water into basin
R	$m^3\ s^{-1}$	River discharge
S_b	$g\ kg^{-1}$	Salinity of basin water
S_o	$g\ kg^{-1}$	Salinity of ocean water
S_{ref}	$g\ kg^{-1}$	Reference salinity used in equation of state of seawater (38.6)
S'	–	Dimensionless basin salinity, $S' = S_b/S_o$
T_{atm}	°C	Atmospheric temperature
T_b	°C	Temperature of basin water
T_o	°C	Temperature of ocean water
T_r	°C	Temperature of river water
T_{ref}	°C	Reference temperature used in equation of state of seawater (13.7 °C)
t	s	Time
t'	–	Dimensionless time, $t' = t\ e/h$

2. Water and salt fluxes: dynamic model with constant forcing

Taking the basin to be in steady state in terms of water volume and salt content, it is possible to derive expressions that relate the water

Table 1
Data on present-day semi-enclosed basins of the Mediterranean region and Middle East. Key to notes: a: 1 Sv = $10^6\ m^3 s^{-1}$; b: calculated from TerrainBase DEM by Meijer and Krijgsman (2005); c: Schroeder et al. (2012); d: Jordà et al. (2017); e: Bryden and Stommel (1984); f: MEDAR/Medatlas 2002 in Rogerson et al. (2012); g: Pinardi et al. (2015); h: calculated from MEDAR/Medatlas 2002 (MEDAR Group, 2002); i: Macdonald et al. (1994); see caption to Fig. 5; j: Criado-Aldeanueva et al. (2012); k: Yari et al. (2012); l: calculated from GEBCO_2014 Grid, version 20,150,318, http://www.gebco.net; m: Verri et al. (2018); n: Maggiore et al. (1998); o: Özsoy and Ünlüata (1997); p: inferred from Falina et al. (2017); q: Biton and Gildor (2011); r: Biton and Gildor (2014); s: Ben-Sasson et al. (2009); t: Sofianos and Johns (2017); u: Smeed (2004); v: Sofianos et al. (2002); w: Johns et al. (2003).

	A	h	Q_b	S_o	S_b	e	T_o	T_b	H
	$\times 10^{12}\ m^2$	m	Sv (a)	$g\ kg^{-1}$	$g\ kg^{-1}$	m/yr	°C	°C	$W\ m^{-2}$
Mediterranean Sea	2.5 (b)	1502 (b)	0.8 (c,d)	36.5 (e)	38.5 (f)	0.7 (g)	16.5 (h)	12.9 (f)	-5.2 ± 1.3 (i)
Med. Sea, alternative (j)	–	–	0.78 ± 0.05	–	S'=1.046	0.442 ± 0.63	15.6 ± 1.1	13.25 ± 0.07	-3.2 ± 1.5
Adriatic Sea	0.14 (k)	244 (l)	0.3 (c)	39.1 (c)	38.58 (c)	−0.69 (m)	15.66 (k)	13.43 (k)	-36 ± 153 (k)
Adr. Sea, alternative	–	–	–	–	–	–	–	–	−17 (n)
Black Sea	0.42 (o)	1262 (o)	Q_o=9.506 × 10^{-3}(o)	35.5 (o)	17.9 (o)	−0.7 (o)	13.5 (p)	–	–
Gulf of Aqaba/Eilat	3.2×10^{-3} (l)	644 (l)	0.0185 (q)	40.4 (r)	40.7 (r)	1.7 (s)	23.2 (r)	21.6 (r)	−55 (q)
Gulf of Suez	9.233×10^{-3} (l)	38 (l)	–	–	–	2.21 (t)	–	–	−58.5 (t)
Red Sea	0.451 (u)	491 (l)	0.37 (v)	36.8 (v)	39.5 (v)	2.06 ± 0.22 (v)	26.5 (v)	23.8 (v)	-11 ± 5 (v)
Persian Gulf	0.239 (w)	34 (l)	0.15 ± 0.03 (w)	37 (w)	39.1 (w)	1.68 ± 0.39 (w)	27.3 (w)	24.5 (w)	-7 ± 4 (w)

fluxes through the strait to the salinities of the in- and outflow. Expressions that were derived for a generalised context by Knudsen (1900), were applied to the Strait of Gibraltar by Nielsen (1912). But, as pointed out by Bryden et al. (1994), the principle was applied to this strait already by Buchanan (1877). The Knudsen relations figure in many courses on (paleo)oceanography as an elegant illustration of the application of conservation laws. Here, we adopt as our starting point the equation that describes the time rate of change of salt mass in the basin of which the steady-state solution is a special case. Combining this with the expression for water volume conservation and a simple parametrisation of strait flow, we arrive at a basic but useful dynamic model. This is here formulated in terms of dimensionless variables to gain insight into the interplay of the contributing factors.

2.1. Theory

The time rate of change of salt mass contained by the basin obeys the following expression

$$\frac{d\,Ah\rho_b S_b}{dt} = Q_o\rho_o S_o - Q_b\rho_b S_b \tag{1}$$

where A is basin surface area [m^2], h is average basin depth [m] and t is time [s]. Basin-water density and salinity are written ρ_b [kg m^{-3}] and S_b [−]. These, just like basin temperature introduced later, must be considered properties averaged over the volume of the basin. Subscript "o" is used to identify the equivalent variables for the ocean. Q_b [$m^3\ s^{-1}$] is the volume flux of the water flowing out from the basin; Q_o [$m^3\ s^{-1}$] that of the inflow from the ocean. Salinity is taken to be expressed in grams of salt per kilogram of water (parts per thousand) and is thus dimensionless. Eq. (1) assumes that river discharge, evaporation and precipitation advect no salt. We now make the common assumption that the densities are similar enough to divide them out of the equation (see discussion below Eq. 7). Then, with Ah constant, we can write

$$A\,h\,\frac{dS_b}{dt} = Q_o S_o - Q_b S_b \tag{2}$$

The same simplification as to density turns the principle of conservation of water mass into a statement of conservation of water volume

$$Q_o + R = Q_b + (E - P)A \tag{3}$$

where R is river discharge [$m^3\ s^{-1}$], E is rate of evaporation [m s^{-1}], and P is rate of precipitation [m s^{-1}].

Introducing $e = (E - P) - R/A$ as the rate of net evaporation per unit area of basin surface (in m s^{-1} and positive when the basin loses water) we can write

$$Q_o = Q_b + e\,A \tag{4}$$

Although much more comprehensive theories for the dynamics of flow through sea straits have been developed (Pratt and Whitehead, 2008; see Rohling et al., 2008, Meijer, 2012 and Simon and Meijer, 2015 for applications to the Miocene Mediterranean) we deliberately focus on the essence, being the notion that flows are determined by horizontal pressure gradients—which in their turn result from density contrasts. Specifically, the deep flow in the strait is taken to be controlled by the difference in density between the water on both sides. Ignoring the role of temperature (see Section 5 though), the density is proportional to salinity and we can write

$$Q_b = c\,(S_b - S_o)^{\frac{1}{2}} \text{ when } S_b \geq S_o \tag{5}$$

and

$$Q_o = c\,(S_o - S_b)^{\frac{1}{2}} \text{ when } S_b < S_o \tag{6}$$

thus depending on whether it is Q_b or Q_o that furnishes the deeper of the two flows. The coefficient c will be referred to as the strait efficiency and has units [$m^3\ s^{-1}$]. The square-root dependence on the density/salinity difference is appropriate for short and narrow straits (such as present-day Strait of Gibraltar) which are in a state of hydraulic control. For wider straits, the Coriolis force balances the along-strait pressure gradient and the dependence on density/salinity proves linear (Whitehead, 1998).

Concentrating on the square-root relationship and the case that $S_b \geq S_o$, the Eqs. (2), (4) and (5) can be combined to yield

$$A\,h\,\frac{dS_b}{dt} = -c(S_b - S_o)^{\frac{3}{2}} + eAS_o \tag{7}$$

This can be used to calcute the evolution of basin salinity under a given ocean salinity and forcing (net evaporation e and strait efficiency c) and forms the basis of our model analyses of the Messinian Salinity Crisis (Meijer, 2006; Topper and Meijer, 2013, 2015). If we retain the densities in the statements for water and salt conservation, we arrive at essentially the same equation, but for a basin-salinity dependent term multiplying the left-hand side. This term changes nearly linearly from 1.03 at $S_b = 35$ to 1.21 when $S_b = 350$ (halite saturation; values calculated with the parameters of the equation of state introduced in Section 5.1), has at most a small effect on the evolution of basin salinity and does not affect the steady-state value.

A generic model for semi-enclosed seas can be obtained by making the governing equation dimensionless. To this extent we introduce $S' = S_b/S_o$ and $t' = t/\tau$ with τ an as yet unknown characteristic time scale. After also dividing all terms by AhS_o we arrive at

$$\frac{dS'}{dt'} = -\frac{c\,S_o^{1/2}\tau}{Ah}(S' - 1)^{\frac{3}{2}} + \frac{e\,\tau}{h} \tag{8}$$

Consideration of the last term suggests that a natural definition of $\tau = h/|e|$. Although in the steady state, the case with $S_b \geq S_o$ is always associated with a positive e, we must also allow for the transient case with elevated basin salinity under a freshwater input from the atmosphere, i.e. $e < 0$. The time scale τ is thus the time it would take to either completely desiccate or fill the basin with the atmospheric flux. Introduction of this time scale yields

$$\frac{dS'}{dt'} = -\left|\frac{c\,S_o^{1/2}}{A\,e}\right|(S' - 1)^{\frac{3}{2}} + \frac{e}{|e|} \tag{9}$$

in which we made use of the fact that c, S_o and A are always positive. The last term, of course, simply reads either +1 or −1. A single dimensionless ratio $c\,{S_o}^{1/2}/A\,e$ which takes its sign from e, is thus seen to determine the solution for dimensionless basin salinity as a function of dimensionless time. This ratio can be thought of as one between two volume fluxes of water and will henceforth be referred to as the "water-flux ratio". The denominator holds the volume flux of water to the atmosphere or vice versa, the numerator represents the strait exchange. To be exact, the numerator equals the outflow for the case that the basin has exactly twice the salinity of the ocean (see Eq. 5). In the case of no strait exchange $c = 0$, and with $e > 0$, the salinity rise of the basin is maximal, $dS'/dt' = 1$. In the more general case with exchange, the negative first term on the right-hand side of (9) represents the reduction in the rise of salinity caused by the swapping of waters between basin and ocean.

An equivalent derivation can be done for the case that $S_b < S_o$ (using Eq. 6). The dimensionless equation then reads

$$\frac{dS'}{dt'} = \left|\frac{c\,S_o^{1/2}}{A\,e}\right|(1 - S')^{\frac{3}{2}} + \frac{e}{|e|}S' \tag{10}$$

When $c = 0$ and with $e < 0$, the second term on the right is negative and salinity is seen to drop at the maximum rate. Any exchange tempers this decrease (first term on the right being positive now that $S' < 1$). Starting from a linear dependence between strait flow and the salinity difference, we arrive at expressions similar to (9) and (10) but with ${S_o}^{1/2}$ replaced by S_o and the exponent 3/2 replaced by 2.

2.2. Application 1: general characteristics

For the case that $S_b > S_o$ Eq. (9) yields an exact solution for the steady state. In this situation the exchange of water and salt with the ocean and the net evaporation ($e > 0$) are in balance such that the basin stays at a constant salinity. Setting $dS'/dt' = 0$, it follows that

$$S' = 1 + \left(\frac{c\, S_o^{1/2}}{A\, e} \right)^{-\frac{2}{3}} \tag{11}$$

This result immediately informs us of the somewhat counterintuitive fact that the steady-state salinity is independent of basin depth (the time needed to reach that steady state certainly is dependent on depth, see below). Also, a reduction in basin surface area, assuming the rate of net evaporation e to be constant, requires an equal reduction of the strait efficiency if the basin is to maintain at the same salinity. If the strait efficiency is also constant, the water-flux ratio (term in brackets) will increase, exchange wins from net evaporation and the salinity settles closer to the oceanic value, i.e. S' is closer to 1.

Eq. (11) is illustrated in Fig. 2 where it is combined with the steady-state solution for $S_b < S_o$ and thus for negative values of the water-flux ratio. For the latter case no exact solution was found and the result is calculated by numerical integration. Also shown in Fig. 2 are the solutions obtained starting from a linear dependence between strait flow and the basin-to-ocean salinity difference. Note that this entails more than predicting a different S' for a given water-flux ratio since the very definition of the water-flux ratio is now different. Fig. 2 shows that basin salinity is close to the oceanic value for most of the range of the water-flux ratio. When the ratio is positive and approaching zero, S' rises asymptotically. When the water-flux ratio approaches zero from the negative end, the limit lies at $S' = 0$, the basin only exporting water to the ocean and filled with river discharge/precipitation of zero salinity.

When we recall that gypsum and halite start forming at, respectively, about 3 and 10 times concentration of normal seawater (i.e., $S' = 3$ or 10), Fig. 2 illustrates once more how extreme the conditions leading to evaporite deposition really are: these concentrations require very small water-flux ratios. The figure also shows how strongly nonlinear the response to restriction is. Even in the case that tectonics and/or sea-level fall result in a gradual restriction and the water-flux ratio decreases at a constant rate, the basin salinity will reach a point where it rises exponentially. The implication is that even a gradual cause will most likely result in an event-like expression in the sedimentary record: for example a sudden change in faunal composition and lithology (cf. Meijer, 2012).

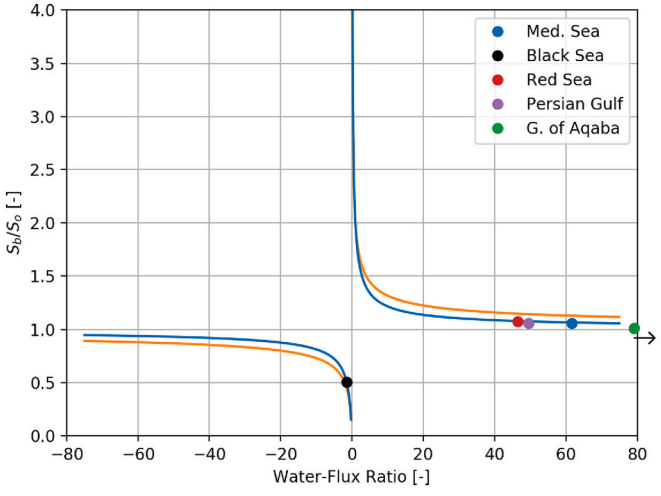

Fig. 2. Relation between water-flux ratio and steady-state dimensionless basin salinity ($S' = S_b/S_o$). Blue line is for a square-root dependence of deep flow in the strait to the salinity difference between basin and ocean; orange line for a linear dependence. Points corresponding to extant basins (Table 1) are superimposed; these are to be compared to the blue line. The green dot for the Gulf of Aqaba/Eilat sits much more to the right at a water-flux ratio of 1245. (For interpretation of the references to colour in this figure legend, the reader is referred to the web version of this article.)

Before applying the graph further to the past of the Mediterranean Sea it is illustrative to know where the extant basins would plot. Table 1 presents a compilation of data from semi-enclosed basins in the Mediterranean region and the Middle East. With Eqs. (5) and (6), i.e. for a square-root relationship between strait flow and salinity difference, we first calculate the strait efficiency coefficient and then use this value to determine the water-flux ratio. The latter is combined with the observed S' to find each basin's position in Fig. 2. The Mediterranean Sea, Red Sea and Persian Gulf exemplify the concentration basins with S' between 1.05 and 1.07. The Gulf of Aqaba/Eilat has a salinity that is only just above that of its "ocean" (the Red Sea) and sits on the asymptote at a water-flux ratio of 1245. The Black Sea represents the dilution basins with a water-flux ratio close to zero. For our purposes, the match between observed properties and the theoretical prediction is certainly fair. The most recent estimate of the outflow through the Strait of Gibraltar due to García-Lafuente et al. (2021) would move the dot for the Mediterranean Sea slightly towards the right, improving the match. In general, any misfit is perhaps due in particular to the observations not reflecting a steady state condition or to the simplicity of our strait flow equation. The Adriatic Sea is not shown because for this basin equating density to salinity in the expression for strait flow is not appropriate. Salinity of the Adriatic basin is less than that of the Mediterranean Sea but the basin still produces a deep outflow through the Strait of Otranto because of the effect of temperature (Verri et al., 2018). This will be the topic of Section 5.3. An additional reason for not including the Adriatic basin is that exchange at the Strait of Otranto is not a simple two-way flow (Astraldi et al., 1999).

As pointed out, the steady-state solution depicted by Fig. 2 is independent of basin depth—depth h only playing a role in the scaling of time. The (dimensionless) time required to achieve equilibrium for a given value of the water-flux ratio is shown in Fig. 3. This is calculated numerically as the time that it takes the basin to reach steady state, from an initial condition of $S' = 1$ (i.e., the basin starts out filled with water of oceanic salinity) and under constant forcing (constant water-flux ratio). Steady state is taken to be reached when the change of S' between two consecutive time steps (10^{-3}) is less than 10^{-5}.

Fig. 3 shows a strongly nonlinear relationship between the water-flux ratio and the time-to-equilibrium. The required time increases greatly for basins for which the exchange with the ocean is small compared to the net volume flux to/from the atmosphere. While the restriction from

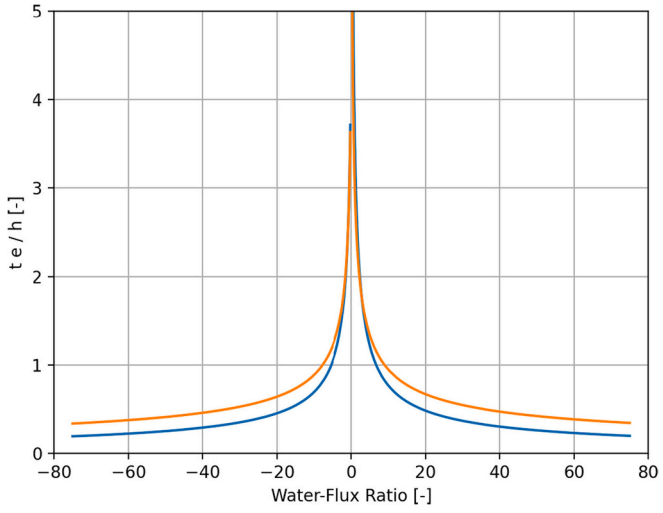

Fig. 3. Time to reach the steady states depicted in Fig. 2, expressed in terms of dimensionless time ($t' = t\, e/h$). Meaning of line colour the same as in Fig. 2.

the ocean implies that the basin will settle at a salinity that is distinct from that of the ocean, that same restriction also slows down the salt import (or export, when the water-flux ratio is negative) required to get there. Looking only at the graph of S' (Fig. 2) it would seem that a simple change in sign of the water-flux ratio results in an extreme response of basin salinity. Because this is the regime in which time-to-equilibrium is very long, this response will in reality (in actual years) be drawn out over a very long period, unless the basin is very shallow.

To clarify the meaning of the dimensional time depicted in Fig. 3 we take the example of the Mediterranean Sea. The water-flux ratio equals 62 and dimensionless time-to-equilibrium is calculated to be 0.226. Combined with $h = 1502$ m and $e = 0.7$ m/yr, this is equal to 485 yr. If the basin were, say, a factor 3 less deep, the actual time-to-equilibrium would be less by the same factor. A smaller basin area would, all other variables staying unchanged, imply an increase of the associated water-flux ratio and a reduction in both the dimensionless and actual time to equilibrium. While noting that time to equilibrium as defined here is not the same as residence time (basin volume divided by volume flow rate), it clearly does form a measure for the time the basin needs to respond to a change in forcing. The water properties of a shallower and/or less extensive basin will adjust faster to, for example, a change in the rate of net evaporation. The opposite is true for a restricted basin where the water properties and, as a consequence, the sedimentary expression of the climatic variability, may lag behind the forcing. This is further explored in Section 3.

Finally, to inform discussions of the Messinian Salinity Crisis (MSC), we quantify the maximum rate of salinity increase and the time that it implies is needed to reach saturation for gypsum and halite. As expressed by (9) the maximum rate of salinity increase occurs when there is no exchange and is then given by $dS'/dt' = 1$. This is easily integrated starting from ocean salinity, i.e., $S' = 1$ to find S' as a function of time. Given that $t = t'\ (h/e)$ and with h and e for the Mediterranean as before, we calculate that gypsum saturation is reached in about 4.3 kyr and halite saturation in roughly 19.3 kyr.

2.3. Application 2: marginal basins during the gypsum stages of the MSC

If we consider a basin that communicates with the ocean or with another basin at normal salinity then, as just mentioned, $S' = 3$ roughly corresponds to the point where the basin achieves saturation for gypsum. For a basin at steady state it follows from Fig. 2 that the water-flux ratio must be small. The analytical solution readily gives the exact value of 0.35. Compared to the present-day Mediterranean Sea this is a reduction of the water-flux ratio by a factor 100. Assuming net evaporation unchanged, this reduction must be achieved by a reduction of the strait efficiency.

Now let us consider the case of the marginal basins within the Mediterranean: semi-enclosed sub-basins of the larger Mediterranean Sea. The Mediterranean then constitutes the "ocean" and we examine the situation in which it is assumed to stay at normal ocean salinity (36 g kg^{-1}). To achieve $S' = 3$ in a basin that occupies a surface area comparable to the present Adriatic or Aegean seas (area of order 10^{11} m^2; see Table 1), while taking net evaporation at 1 m/yr, the strait efficiency is found to equal 6654 m^3 s^{-1}. For all their limitations, reconstructions of the marginal basins that accumulated gypsum during the MSC point to smaller surface area of order 10^9 m^2 (Modestou et al., 2017, for the Sorbas basin; Natalicchio et al., 2019, for Piemonte basin; Manzi et al., 2012, for the Caltanissetta basin). In this case the strait efficiency associated with a water-flux ratio of 0.35, making the same assumptions as before, is equal to 67 m^3 s^{-1}, which is a factor 10^4 smaller than the efficiency of present Strait of Gibraltar. Even though it now multiplies the relatively large difference in salinity between a basin at gypsum saturation and one at oceanic salinity (Eq. 5), such a reduced strait efficiency corresponds to a small exchange flux, of order 10^3 m^3 s^{-1}. This is the order of magnitude of the discharge of the large rivers flowing at present into the Mediterranean Sea. Although we cannot exclude the possibility, it seems unrealistic to assume that the marginal basins accumulated their gypsum deposits because they had such very limited exchange with a main Mediterranean basin at normal salinity. More likely, the main basin sourced the marginal basins with water at already elevated salinity because it was itself restricted from the Atlantic Ocean. These theoretical results lend support to the objection of de De Lange and Krijgsman (2010) against the silled-basin explanation for Stage 1 of the MSC (Roveri et al., 2008).

3. Water and salt fluxes: dynamic model with variable atmospheric forcing

Staying with the same basic principles we now focus on time-dependent behaviour. More precisely, we examine the response to periodic climatic forcing.

3.1. Theory

The general behaviour of a semi-enclosed basin in response to periodically-varying atmospheric forcing can be examined by writing the net evaporation as a sine-function of time.

$$e = e(t) = e_m + e_a sin\left(2\pi\ \frac{t}{p}\right) \tag{12}$$

in which e_m is the mean net evaporation [m s^{-1}], e_a the amplitude [m s^{-1}] and p the period [s] of variation. Let $t' = t/\tau$ with now $\tau = h/|e_m|$ then the dimensionless Eq. (9) becomes

$$\frac{dS'}{dt'} = -\left|\frac{c\ S_o^{1/2}}{A\ e_m}\right|(S' - 1)^{\frac{3}{2}} + \frac{e_m}{|e_m|} + \frac{e_a}{|e_m|} sin\left(2\pi\ \frac{t'}{p'}\right) \tag{13}$$

where

$$p' = p/_\tau = p\ |e_m|/_h \tag{14}$$

and, of course, $t'/p' = t/p$. In the same way an equation can be derived for the case of a linear dependence between strait flow and the basin-to-ocean salinity difference. The governing Eq. (13) does not yield easily to analytical solution. One would expect a solution of the form

$$S'(t') = \langle S' \rangle + \Delta S' sin\left(2\pi\ \frac{t' - \Delta t'}{p'}\right) \tag{15}$$

in which $\langle S' \rangle$ is the long-term average of S', $\Delta S'$ its amplitude of variation and $\Delta t'$ the dimensionless duration of any offset relative to the forcing. While numerical integration demonstrates that the resulting time-dependent basin salinity is not, at least not always, such a perfect phase-shifted and scaled version of the forcing function, it closely resembles this in most cases. In the results presented below, the integration is always continued long enough for the basin to reach a dynamic steady state in which each new cycle is the same as the preceding one. The amplitude of variation of S' is then determined, as well as the dimensionless time lag between forcing and basin salinity (calculated as the average offset of the extrema).

3.2. Application 3: generalised response to periodic forcing

Some relevant insight regarding the response to variable forcing can be inferred directly from the equations. Firstly, as for the case of constant forcing, if two basins subject to the same forcing also have the same water-flux ratio and basin depth, their response in terms of S' will be the same. Secondly, when the period of variation and basin depth are both multiplied by the same factor, the result remains the same (Eq. 14). For example, for a given mean and amplitude of net evaporation, variation over 100 kyr, imposed on a 1500 m deep basin, gives the same

amplitude of variation of S' as a 20-kyr variation acting on a 300 m deep basin. The two situations correspond to the same p'. Thirdly, reduction of basin area alone, will decrease, not increase, the response to a given forcing. As already encountered in the discussion of (11), a reduction of basin area corresponds to an increase of the water-flux ratio which means that basin salinity stays closer to that of the ocean.

Fig. 4 summarizes the results of a large number of calculations for the case that net evaporation is always positive (a water loss) and $e_a/e_m = 1/6$. To provide some reference: the latter value would be appropriate for the precessional cycle of the Mediterranean basin (Dirksen and Meijer, 2020). The top panel shows that the amplitude of S' is negligible when the water-flux ratio is large. For smaller values of the water-flux ratio, the amplitude is found to first increase with increasing period of variation and then level off at a maximum. This levelling off occurs at ever longer periods when water-flux ratio is reduced; for a water-flux ratio of 0.05 the maximum is attained beyond the range of our figure. Although not shown, the amplitude is found to scale roughly linearly with the amplitude of the forcing while the overall behaviour is unaffected.

The effect of the water-flux ratio on amplitude is as expected given the results for constant forcing presented in the previous section. With relatively short periods of variation, the basin is not given sufficient time to adjust to the forcing and the maximum S' is below the value which would be attained if the net evaporation was kept constant at its maximum (and likewise for the minima). For longer periods of variation the basin is essentially always in equilibrium with the forcing and the amplitude is dependent only on the amplitude of the variable net evaporation. Because a more restricted basin takes longer to adjust to forcing (see Fig. 3), the period at which the amplitude levels off is longer in the case of a smaller water-flux ratio.

Focussing now on the lag between forcing and response it is best to view a plot of dimensionless lag divided by dimensionless period, i.e., the phase shift expressed as a fraction (Fig. 4, bottom panel). A graph of dimensionless lag itself as a function of period (which proves very similar to that of amplitude) is not easily queried for the role of basin depth or mean net evaporation because these variables would then enter in *both* axes of the diagram in the form of the scale for time. Fig. 4 indicates that the lines for different values of the water-flux ratio converge at a phase shift of a quarter period when the period approaches zero. This quarter period is the phase shift expected for a basin without exchange with the ocean. In this case, a one-way flux from the ocean varies in pace with net evaporation. The implied sine function of the incoming

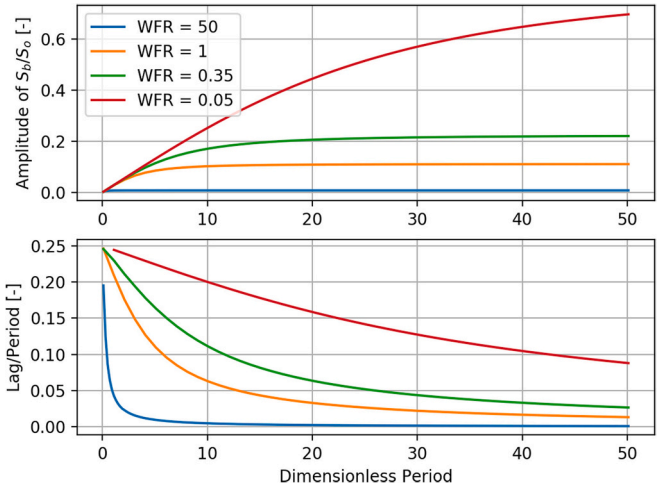

Fig. 4. Generalised response of a semi-enclosed basin to periodically varying freshwater forcing where the ratio between the amplitude of the forcing and its mean is 1:6. As a function of the dimensionless period of the forcing on the horizontal axis, the top panel gives the amplitude of S' ($\Delta S'$ of Eq. 15) and the bottom panel its dimensionless lag (i.e., phase shift; $\Delta t'/p'$). Lines correspond to indicated values of the water-flux ratio (WFR).

salt flux integrates to a negative-cosine function (i.e, a sine shifted by $\pi/2$ or one quarter period) for salt content, plus a constant increase in time related to the mean of net evaporation. For the case of a large water-flux ratio (blue line in Fig. 4) the phase shift drops to 0 as soon as the period of variation is increased. With smaller values of the water-flux ratio, the decrease of the phase shift is spread out over a longer range of periods and the minimum attained lies above 0.

The result that the lag, expressed as a phase shift, decreases with increasing period of variation is understood from the fact that, as already pointed out above, a slower variation gives the basin more opportunity to achieve equilibrium with the forcing. The minimum phase shift attained for longer periods of variation expresses the limit on the salt flux into or out of the basin exerted by the gateway. The more restricted the gateway, the closer the phase shift sits to the quarter-period lag associated with a basin completely without exchange. The overall shape of these curves has a general implication for the practice of astronomical tuning of sedimentary sequences in a semi-enclosed basin. To the extent that different periodicities of the forcing are reflected in the sedimentary succession via salinity, it follows that any lags between the forcing and the record (lithology, faunal composition, isotopic or other aspects of chemical make-up) may not be the same for each forcing frequency.

3.3. *Application 4: precessional variation of the Mediterranean Sea*

To make the results more concrete we consider the case of precessional variation acting on the present-day Mediterranean basin. We have $p = 21$ kyr, $h = 1502$ m and $e_m = 0.6$ m/yr. The latter value, in combination with $e_a = 0.1$ m/yr, gives as a maximum the presently observed net evaporation (Table 1). This is consistent with the notion that the present orbital configuration is close to a precession maximum and represents the most arid stage of the precessional cycle (cf. Dirksen and Meijer, 2020). With these three values we calculate that the dimensionless period $p' = 8.4$. It then follows from Fig. 4 that, under present-day conditions (water-flux ratio = 62), both amplitude and phase shift of the response of the basin in terms of basin-averaged salinity are negligible. If, in contrast, the same basin sits at 3 times concentration (i.e., gypsum saturation; water-flux ratio = 0.35), the amplitude of S' is clearly below that which would be achieved in steady state. More notably, the basin would exhibit a significant lag: a phase shift of 0.125 corresponding to 2.6 kyr. While this latter value is below the resolution of astronomical tuning it does mean that it is incorrect to take the middle of a gypsum bed to coincide with a peak in insolation (e.g., Manzi et al., 2013). This may have consequences for the interpretation of the sequence of facies or their geochemical properties within a precession cycle, in terms of the underlying mechanism (Lugli et al., 2010). The lag expected between gypsum and insolation has been previously addressed from the point of view of modelling by Topper and Meijer (2015) who also evaluate whether it affects the estimates for the start of the Messinian Salinity Crisis (it most likely does not). Going beyond our previous modelling, Fig. 4 further demonstrates that, for a basin at 3 times concentration and in comparison to the response to precession, the phase shift associated with obliquity (about 40 kyr) and eccentricity (about 100 kyr) are much shorter. The latter illustrates the general behaviour pointed out at the end of the previous section.

When we focus on a shallower basin, say $h = 200$ m, the same net evaporation translates the period of the precessional cycle to a dimensionless equivalent $p' = 63$. It then follows from Fig. 4 that the amplitude is maximal while the phase shift is minimal: also at gypsum saturation a shallower basin is able to keep pace with the precessional forcing much more closely than a deep basin does. However, if that shallow basin reached 3 times concentration (with respect to its "ocean") under a net evaporation that on average sits much closer to a neutral water budget (say, $e_m = 0.1$ m/yr), the corresponding dimensionless period $p' = 10.5$ and the lag between response and forcing is again found to be significant.

4. Heat fluxes added: budget considerations

In this section the principles of conservation of water and salt are complemented with the conservation of heat. At first, we do without a dynamic representation of strait flow and only consider the issue of budgets. The three conservation statements are combined into a single expression that describes a semi-enclosed basin in a state of constant volume, salinity and temperature.

4.1. Theory

When the basin water is of constant temperature, conservation of heat implies a balance between heat input into the basin and heat output from it and can be written (e.g., Tziperman and Speer, 1994; Criado-Aldeanueva et al., 2012),

$$Q_o T_o + R T_r + HA/\rho C_p = Q_b T_b + (E-P) A T_b \tag{16}$$

in which T_o and T_b are the temperatures of ocean and basin, respectively, and T_r that of the river water. H is the heat flux from the air to the basin water in Wm^{-2}, positive when heating the water. In writing (16) we approximated the temperature of the precipitation by that of the basin waters. Also, a single average reference density ρ_{ref} is combined the specific heat C_p to convert from temperature to heat and vice versa. In the calculations below we use $\rho_{ref} = 1029$ kg m^{-3} and $C_p = 3990$ J kg^{-1} °C $^{-1}$.

Approximating also the river-water temperature by that of the basin and using, as before, $e = (E-P) - R/A$ as the rate of net evaporation (introduced below Eq. 3) we can write

$$Q_o T_o + HA/\rho_{ref} C_p = Q_b T_b + e\, A\, T_b \tag{17}$$

The last term represents the heat that is taken out of the basin by the net evaporative flux. It should not be confused with the latent heat of evaporation which is contained in H and is much larger. For example, for the present-day Mediterranean Sea, $e\rho C_p T_b$ amounts to 1.2 Wm^{-2} while the annual and basin mean latent heat loss is estimated at 98 Wm^{-2} (Song and Yu, 2017). It is important to retain the term because without it, the case that $H = 0$ while net evaporation is non-zero such that $Q_o \neq Q_b$, would give the unphysical result that $T_o \neq T_b$.

Combining water conservation (4) and salt conservation (Eq. 2, for the steady state) we obtain one form of the Knudsen relations

$$Q_b (S_b - S_o) = eAS_o \tag{18}$$

Q_b represents the volume flux that in- and outflow have in common and thus gives the magnitude of the true exchange flux. Also, eA is the volume flux to the atmosphere (focussing on an evaporative basin) and is equal to the net inflow of water. Eq. (18) can thus be read as saying that "exchange-related salt loss = salt gained by net inflow". An equivalent statement for heat is found by combining water conservation (4) and heat conservation (16)

$$-Q_b (T_b - T_o) = eA(T_b - T_o) - HA/\rho_{ref} C_p \tag{19}$$

In (other) words, "exchange-related heat gain = heat lost with net evaporation - heat gained by net inflow - heat gained from atmosphere". Where, of course, strictly speaking we should have written gain or loss of "temperature" rather than "heat". Dividing all terms through $eA(T_b - T_o)$ and using Eq. (18) to substitute for Q_b we readily obtain

$$\frac{H}{e\,(T_b - T_o)\,\rho_{ref} C_p} = \frac{1}{1 - 1/S'} \tag{20}$$

where $S' = S_b/S_o$, as before. The left-hand side represents the dimensionless ratio between the air-sea heat flux and the fluxes set by the rate of evaporation. From now on I will refer to this term as the "heat-flux ratio". The right-hand side is proportional to the state of basin restriction. Note that this expression has been derived without making assumptions about the dynamics of strait flow, it purely embodies conservation of water, salt and heat.

4.2. Application 5: why is the net air-sea heat flux of the Mediterranean Sea small?

Although its determination is wrought with uncertainty, the annual-mean basin-averaged net flux of heat between the Mediterreanean Sea and the atmosphere is inferred to amount to a loss by the basin of ~4–5 Wm^{-2} (Macdonald et al., 1994; Jordà et al., 2017). This value is small in comparison to the seasonal variation of the basin-averaged net heat flux of about ±150 Wm^{-2} (Criado-Aldeanueva et al., 2012; Song and Yu, 2017). The value is also smaller than the spatial variation of the annual-mean net heat flux of roughly ±30 Wm^{-2} (Tsimplis et al., 2006; Song and Yu, 2017). The very fact that the Mediterranean basin is large enough to encompass both regions that gain and lose heat on an annual basis will be at least part of the explanation for the limited mean value. Also, that the basin must lose heat to the atmosphere on an annual mean basis is understood from the fact that its intermediate and deep waters are formed in winter, "sampling" cold surface conditions and it is these relatively cold waters that flow out at Gibraltar. The lower temperature and lesser volume transport of the outflow compared to the inflow imply that the basin gains heat at its ocean connection, heat that must be lost to the atmosphere. Do the combined conservation equations of water, salt and heat provide further clues?

The term on the right-hand side of Eq. (20) is plotted in Fig. 5 as a function of S'. Whereas in preceding sections S' was the unknown which we set out to calculate as a function of the forcing, here it is plotted on

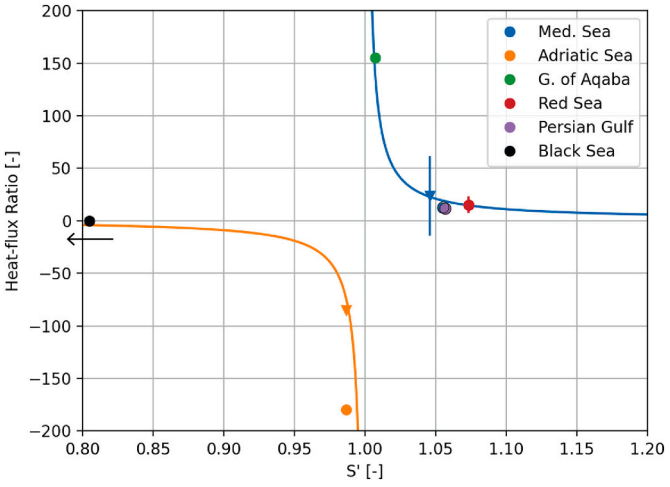

Fig. 5. Graph of the heat-flux ratio as a function of S'(Eq. 20), with points corresponding to extant basins superimposed (Table 1). Uncertainties in the heat-flux ratio are shown where error estimates are available. For the Persian Gulf these are so small they fall behind the dot. The blue dot (falling largely behind the symbol for the Persian Gulf) refers to the Mediterranean Sea using the Macdonald et al. (1994) heat-flux estimate. The latter concerns the total heat advected through the strait and must therefore be reduced by an amount eT_b to be comparable to our H. Without this reduction the symbol shifts slightly closer to the curve. All other strait-advection based estimates of H were found to to be already adjusted in this sense. The blue triangle is for the Mediterranean Sea using the data of Criado-Aldeanueva et al. (2012). The horizontal distance between this and the other estimate for the Mediterranean Sea gives an indication of the uncertainty in S'. The black dot corresponding to the Black Sea is actually situated much more to the left, at $S' = 0.5$. The orange dot for the Adriatic Sea is based on the heat flux estimated by Yari et al. (2012). Its error bar would span the whole graph (not shown). The orange triangle is for the same basin, using the Maggiore et al. (1998) heat-flux estimate. (For interpretation of the references to colour in this figure legend, the reader is referred to the web version of this article.)

the x-axis because we aim to examine the atmospheric forcing (in the form of the heat-flux ratio) as a function of basin restriction, as expressed by S'. Combinations of S' and the value of the heat-flux ratio (i.e., left-hand side of 20) calculated using the observed basin properties, are superimposed. Note that both H and $T_b - T_o$ are negative for all basins except the Black Sea for which H is essentially zero. For our purposes and viewed over the range of the axes in Fig. 5, the match between the theoretical curve and the data is certainly fair. The Mediterranean Sea with the Macdonald et al. (1994) heat-flux estimate and the Persian Gulf plot below the line which corresponds to a true equilibrium. Whether this is due to inadequacy of the data or indicative of on-going change in heat and/or salt content is beyond the scope of this paper. The second point for the Mediterranean Sea is based on Criado-Aldeanueva et al. (2012) and, to be specific, uses their estimate of H obtained from the advection of heat through the strait of Gibraltar. The relatively large uncertainty is due to the uncertainty in the estimate of net evaporation (see Table 1). Integrating instead the air-sea fluxes these authors found an H close to zero which would thus bring the estimate well below the curve in Fig. 5. The difference between the two estimates of H is indeed interpreted by Criado-Aldeanueva et al. (2012) as indicative of on-going warming of the sea.

Fig. 5 illustrates that the heat-flux ratio is relatively small for all but the values of S' very close to unity. Small heat-flux ratios are found for the Mediterranean Sea, the Red Sea and the Persian Gulf. Higher values of the heat-flux ratio are reached when the basin is less restricted. The Gulf of Aqaba/Eilat and the Adriatic Sea demonstrate the situation in which these higher values of the heat-flux ratio are mostly due to a more negative H (see Table 1). The Gulf of Suez also has a large negative heat flux (Table 1) but data are lacking to place this basin in the figure. When S' approaches unity even further, the implied greater exchange flux will also lead to a decrease of $(T_b - T_o)$, causing the heat-flux ratio to respond asymptotically. Moving away from the Mediterranean and similar basins in the opposite direction, that is, towards greater restriction, Eq. (20) predicts the heat-flux ratio to decrease. To be precise, for concentration basins, in the limit as $S' \to \infty$, the heat-flux ratio tends to unity and $H = e\,(T_b - T_o)\,\rho_{ref} C_p$. In other words, in the absence of exchange, the heat flux from the atmosphere makes up for the difference between heat lost with the net evaporation and heat carried in by the inflow from the ocean. For dilution basins approaching disconnection from the ocean, that is as $S' \to 0$, the heat-flux ratio approaches 0. This behaviour is illustrated by the present-day Black Sea ($S' = 0.5$) where heat advection through the Bosphorus is negligible (Garrett et al., 1993). Heat brought in by the excess of river discharge over $E - P$, is exported by the net outflow at the strait. Note that it is in these limits that our assumptions as to the temperature of precitation and river discharge may play a role.

In conclusion, Fig. 5 clearly brings out the role of basin restriction in the heat budget of the semi-enclosed basin. Whereas the relatively small net air-sea heat flux of the Mediterranean Sea will in part be controlled by atmospheric conditions, basin geography and circulation, we are now able to understand it as an expression as its state of restriction as well. The implication for the study of the paleoceanography of the Mediterranean Sea or of other basins is that, if the basin is as restricted as the present Mediterranean or more, one may expect there to be no significant role for the annual mean and basin-averaged heat flux. The role of heat and temperature for semi-enclosed basins is further explored in the next section.

5. Heat fluxes added: dynamic model

Still considering basin volume as constant, we re-introduce a dynamic representation of strait flow and combine this with the equations for the time-rate-of-change of salt and heat.

5.1. Theory

By combining the expressions for conservation of water volume (4), basin salinity through time (2) and the equation for the time rate of change of basin temperature that underlies (16), we obtain a dynamic model that considers both salinity and temperature. This requires we make the deep flow through the gateway a function of the difference between the density of the basin (ρ_b) and ocean (ρ_o), rather than just the difference in salinity (5). For example, when $\rho_b > \rho_o$

$$Q_b = c\,(\rho_b - \rho_o)^{\frac{1}{2}} \tag{21}$$

where the units of c have now changed to the cumbersome $m^3 s^{-1} (kg\ m^{-3})^{-1/2}$ or $m^{4.5} s^{-1} kg^{-1/2}$. This step entails the introduction of an equation of state for which we use a simple linear approximation

$$\rho = \rho_{ref}\left(1 - \alpha\left(T - T_{ref}\right) + \beta\left(S - S_{ref}\right)\right) \tag{22}$$

where the various parameters have been set to values appropriate for the present-day Mediterranean Sea. The reference values are $T_{ref} = 13.7\ ^\circ C$ and $S_{ref} = 38.6$ (ρ_{ref} was already introduced). The thermal expansion coefficient $\alpha = 2 \times 10^{-4}\ ^\circ C^{-1}$ and the haline contraction coefficient $\beta = 7.5 \times 10^{-4}$. In the first application below we replace the imposed heat flux H (see Eq. 16) by a relaxation to a prescribed atmospheric temperature T_{atm} such that

$$H/\rho_{ref} C_p = \gamma\,(T_{atm} - T_b) \tag{23}$$

which has the effect of nudging basin temperature towards the chosen atmospheric value at a rate set by the coefficient γ in $m\ s^{-1}$. This coefficient can be thought of as the depth of the water layer affected by the forcing over a certain amount of time and its value needs to be chosen at the outset, for instance by reference to model studies constrained by observations of the present day.

5.2. Application 6: the effect of temperature

In many situations the effect of temperature on density is subordinate to that of salinity and can be neglected. For example, Bryden and Stommel (1984) argued this to hold true for the dynamics of the Strait of Gibraltar, exactly because the heat flux of the Mediterranean Sea is small (Section 4.2). When the basin is restricted and salinity rises to high values (think of the Mediterranean during the MSC), the neglect of temperature will be only more justified, density being essentially set by salinity. Here we quantify the effect that temperature, through its influence on the density—and thus rate—of the outflow, exerts on basin salinity. Rather than imposing different values of the heat flux we relax the basin temperature to a range of imposed atmospheric temperatures (23) because the latter is easier to interpret.

We focus on a basin with the surface area, depth and net evaporation of the present-day Mediterranean Sea (Table 1). Strait dynamics is included in the form of Eq. (21). From the observed ocean and basin properties we calculate the density difference and next, using (21), the strait efficiency that gives the presently observed magnitude of the outflow is found: $c = 5 \times 10^5\ m^3 s^{-1} (kg\ m^{-3})^{-1/2}$. Starting with the basin at the same temperature and salinity as the ocean we then calculate the evolution of basin temperature and salinity, in response to net evaporation and with relaxation to an assumed air temperature. The relaxation coefficient γ is taken at 1 m/day, as in the OGCM-implementations for the Mediterranean Sea of Drakopoulos and Lascaratos, 1999 and Topper and Meijer, 2015. At the end of the run the steady-state salinity is recorded and the calculation is repeated for a range of atmospheric temperatures. We consider a range of $\pm 5\ ^\circ C$ around the temperature of the outside ocean. To put this in perspective, a $5\ ^\circ C$ increase of basin-averaged temperature would result from an unbalanced heat input of $1\ W\ m^{-2}$ maintained over 1 kyr. The results are depicted in Fig. 6 in terms of the salinity difference relative to solution obtained for an air temperature exactly equal to the temperature of the ocean water.

The effect of variation in the air temperature is very small, as anticipated. It is less, but perhaps surprisingly, not much less, when the

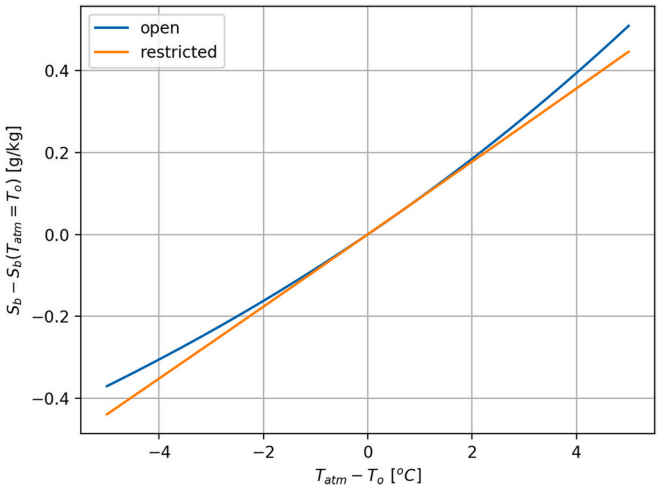

Fig. 6. The influence of atmospheric/basin temperature on basin salinity. Basin temperature is relaxed to a range of atmospheric temperatures, varied around the oceanic value, as given on the horizontal axis. The steady-state basin salinity calculated to correspond to this, is on the vertical axis. Salinity is shown relative to the value that it attains when $T_{atm} - T_o = 0$. The two lines correspond to different degrees of restriction: strait efficiency $c = 0.5 \times 10^6$ m^{3}s^{-1}(kg m^{-3})$^{-1/2}$ ("open", blue curve) and 0.5×10^4 ("restricted", orange). (For interpretation of the references to colour in this figure legend, the reader is referred to the web version of this article.)

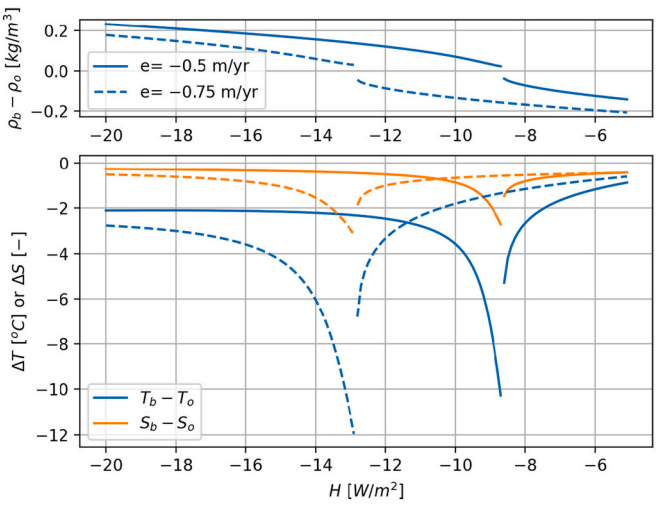

Fig. 7. The effect of heat flux on the properties of a marginal basin to the Mediterranean Sea, subject to cooling ($H < 0$) in combination with net freshwater input ($e < 0$). Solid and dashed lines correspond to two values of the rate of net evaporation. Bottom panel gives, relative to the "oceanic" value, basin temperature (blue) and basin salinity (orange) calculated for the steady state. Top panel illustrates the corresponding density difference. (For interpretation of the references to colour in this figure legend, the reader is referred to the web version of this article.)

calculation is repeated for a restricted basin in which c is reduced by 2 orders of magnitude. The results for both open and restricted basin are essentially unchanged when the relaxation coefficient γ is increased to 1 m/h (not shown). Because the heat flux is a function of both the relaxation coefficient and the evolving basin temperature, an increase in γ does not translate directly to a larger heat flux. It does mean that the coupling between atmosphere and sea is stronger. The relaxation coefficient would play a larger role if the forcing were changing over time.

A more significant role for temperature may occur in situations in which the basin salinity sits very close to the oceanic value. Imagine, for example, a basin that has a small excess salinity. Increased heating of the basin waters may then offset the density effect of salinity and lead to a flow reversal in the gateway, from anti-estuarine to estuarine. The generic model of Section 2 informs us when this could occur: S_b/S_o close to 1 is found when the absolute value of the water-flux ratio is large, that is, for large c (open connection), small surface area A, and small net evaporation e.

5.3. Application 7: a marginal Mediterranean basin subject to freshwater input

An interesting case in point is the present-day Adriatic Sea (Verri et al., 2018). Here the situation is opposite to that sketched at the end of the preceding section: the basin is subject to a net freshwater gain but cooled by the atmosphere, such that exchange is still anti-estuarine. The freshwater gain is significant: its absolute value is equal to that of the net evaporation of the Mediterranean as a whole. At least at present, flows through the Strait of Otranto are more complex than the two-way exchange representation in our model. Apart from a deep dense outflow (value given in Table 1) there occurs a surface outflow of lower-salinity water (Astraldi et al., 1999; Yari et al., 2012). Nevertheless, a generic analysis of the behaviour of this type of marginal basin to the Mediterranean Sea, adopting our idealised strait exchange, proves to offer relevant insight. Note that also the present-day Aegean Sea is thought to combine cooling and freshwater gain (Ashkenazy et al., 2012). Fig. 7 presents a dedicated model calculation. The set-up is roughly tailored to the Adriatic Sea with a surface area of 0.1×10^{12} m^2 and basin depth of 200 m. We apply the linear relationship between strait flow and the density difference appropriate for wider straits and set the strait coefficient c to 1×10^6 m^{3}s^{-1}(kg m^{-3})$^{-1}$. The effect of the latter choice is discussed below. Properties of the "ocean" are roughly those of the present-day Mediterranean Sea: 16 °C and 38 g kg^{-1}. For two different values of the rate of net evaporation (negative and thus an input), Fig. 7 gives the (steady-state) basin temperature and salinity that result for a range of values of the imposed heat loss to the atmosphere. Also shown is the density difference between basin and its "ocean", the Mediterranean proper.

For both values of net evaporation, the solution consists of two branches with a discontinuity that corresponds to the point where the density difference between the two sides of the strait changes sign and the exchange changes from anti-estuarine (positive density difference) to estuarine (negative difference) or vice versa. With $e = -0.5$ m/yr, for heat flux more negative than about -8.6 Wm^{-2}, the cooling is such that the basin has a density excess (see top panel of Fig. 7). With less cooling, the freshwater gain keeps the density of the basin below that of the Mediterranean Sea and exchange at the strait is predicted to be estuarine. Approaching the neutral state at $H = -8.6$ Wm^{-2} from either smaller or larger heat flux values, the basin temperature and salinity are seen to drop. A small density difference means small exchange and the basin properties are then dominated by the cooling and freshening of the basin waters. It is for this same reason that a truly neutral state cannot persist (and the top panel shows a discontinuity). With zero exchange the forcing would cause basin density to move away from the oceanic value again. Time series of the individual experiments that make up Fig. 7 show how, close to the neutral state, the basin properties first approach the values corresponding to the "left branch" of the solution, nearly settle there apart from a small drift, and then suddenly jump to the values of the "right branch".

When the freshwater input is taken larger (e decreased to -0.75 m/yr), the discontinuity is seen to shift to more negative heat flux (dashed lines in Fig. 7). A larger cooling is now required to offset the density decrease due to dilution. When strait efficiency is increased (not shown) the branches of the solution move upwards, reflecting that the basin properties stay closer to those of the ocean, but the position of the discontinuity is hardly affected.

These model results suggest that the properties of a semi-enclosed

sea subject to freshwater gain and cooling may be very sensitive to a change in the heat budget. When the heat loss approaches the point where exchange flips sign, in particular the temperature is expected to decrease significantly. As we first encountered in Section 2, the associated limited exchange does mean that the time to reach these low values is long, of the order of 100–1000 year. For example, would, in the case of $e = -0.5$ m/yr, the heat flux change from -10 Wm^{-2} to -8 Wm^{-2} over a shorter period, there would be a transient drop in temperature and salinity, significant but not as extreme as the steady-state values. Moreover, it is likely that in reality the reduced basin temperature would trigger a response of the air-sea flux while here it is kept constant. In terms of the model representation, the present-day Adriatic Sea would plot to the left of the discontinuity. But whether the behaviour demonstrated here is applicable to this basin and, for example, its response to reduced heat loss in a warming world, remains to be established with a more involved model analysis, respecting the intricacies of the exchange at Otranto.

Considered in the wider context of paleoceanography, the analysis above illustrates how air-sea heat flux may result in a sense of exchange, estuarine or anti-estuarine, unsuspected from the sign of the freshwater budget. It would seem to require proxies on both temperature and salinity, and/or insight into the climatic forcing, to detect this behaviour in the geological past. If, in addition to a reconstruction of basin properties, we have at our disposal proxy records from the vicinity of the strait, this provides an excellent way to establish the overall functioning of the basin. Cores obtained to the west of the Strait of Gibraltar form an example (e.g., Sierro et al., 2020, and references therein) and Incarbona et al. (2011) applied the same logic to the Strait of Sicily. The Adriatic Sea and the Aegean Sea are the source of the deep waters of the present-day eastern Mediterranean and thus an important element of the thermohaline circulation (e.g., Pinardi et al., 2019). It is clear that reconstruction of the past functioning of these basins (e.g., Marino et al., 2007) is essential to understand the evolution of Mediterranean overturning circulation, for example as it is expressed in the sapropel record (Dirksen and Meijer, 2020).

6. General discussion

Early on in the theoretical development we chose to combine river discharge R with $E - P$, into a single rate of net evaporation e (below Eq. 3). This rate is multiplied with basin area to obtain the corresponding volume flux of water. Using e makes for a clean formulation that lends itself well to non-dimensialisation and extension towards inclusion of heat fluxes. The disadvantage is that the volume flux R does not necessarily scale with basin area in the same way as the volume flux due to $E - P$ does. Imagine two adjacent basins, one large and one small, that experience the same $E - P$ per square metre of their surface area. The water budget of the small basin may be dominated by R when a river happens to debouch there. Going from the large to the small basin, the reduction in area is then accompanied by a reduction in e, perhaps even to negative values (net freshwater gain). An example is the Adriatic Sea (with the Po river) compared to the Mediterranean Sea as a whole. How would this affect the insight obtained? Both for constant forcing (Section 2) and in the case of periodic change (Section 3) it was pointed out that reduction of basin area alone will cause the basin to settle at a salinity closer to that of the ocean: the ocean exchange becomes more important than the volume flux due to net evaporation. The remark made here is that reduction in area may well be paired with a change in e, causing basin salinity to still move away from the oceanic va

A comparable limitation to the scaling of the forcing with basin area relates to the air-sea heat flux. As mentioned in the discussion of the reasons for the small magnitude of the annual-mean and basin-averaged heat flux of the Mediterranean Sea (Section 4.2), a small basin is perhaps less likely to compensate heat gain in one part, with a loss elsewhere (the present-day Gulf of Aqaba/Eilat and Gulf of Suez are both a case in point). Hence, in an absolute sense, the integrated heat flux HA for a small basin may be greater than that for a larger basin.

Eqs. (5) and (6) introduced the simplified representation of strait-flow dynamics for the case that salinity is the main control on density. Later, in Section 5, a more general form that also accounts for the effect of temperature was used (21). The strait efficiency coefficient c represents the degree by which water flow is restricted by the very geometry of the strait: width, depth and channel length, in particular. While for the Mediterranean region tectonically-induced changes in strait geometry have been very important, the various geometrical aspects, water depth above the sill most obviously, are also dependent on sea level (Bryden and Kinder, 1991; see below also). Even when geometry and sea level are not changing, a given strait can display a range of "efficiencies", up to a certain limit for which the exchange is maximal (Bryden and Stommel, 1984). The central variable is the position of the interface between in- and outflow. This position (depth) is in part dependent on the circulation within the basin, in particular the degree of mixing between in- and outflow. Thus, for example when we examine a situation that involved significant variation in the degree of mixing within the basin, it may be required to consider a range of c even when tectonics and sea-level change are inactive. Garrett (1996) already pointed out the audacity of assuming the Strait of Gibraltar to always be at its maximal limit. In Meijer (2012) the hydraulic-control model is applied to the Messinian Salinity Crisis, keeping interface depth a variable and thus making explicit its role (in this paper I also provide entries to the vast literature on strait dynamics).

Generally speaking, the role of heat flux and temperature depends very much on the situation at hand. For restricted basins the average heat flux is small and salinity has a larger effect on density than temperature. However, even a small unbalanced heat flux leads to a significant temperature rise or fall when maintained over the time scales of interest to geology. Also, heat flux becomes important for semi-enclosed basins with a near neutral freshwater budget because it may determine the sign of the exchange at the gateway.

Heat flux typically has a much stronger seasonal cycle than the freshwater forcing and sea-surface temperature usually varies strongly throughout the year. It is tempting to ignore this seasonal variation when interest lies with the behaviour of the basin on the long timescale. But the process of deep-water formation—clearly essential in determining the water properties near the seafloor and thus those recorded by the sediment—is typically seasonal (e.g., Tziperman and Speer, 1994, for the Mediterranean Sea). It requires models more advanced than the 1-box set-up of this paper to capture deep-water formation but these models must do justice to its seasonal nature either by following the yearly cycle or by focussing on the season of deep convection (perpetual-winter forcing). With a focus on the formation of sapropels, Matthiesen and Haines (2003) and Dirksen and Meijer (2020) developed dynamic box models that represent aspects of the thermohaline circulation. In the latter paper we show that precessional variation of the temperature forcing contributes to switching the basin in and out of organic-rich deposition.

Whereas salinity and temperature were allowed to change with time, in all the analyses we assumed a steady state for basin volume. Sea level change will play a role when we consider the response to the glacial cycle. With a lower sea level the strait becomes effectively less deep and thus less efficient (e.g., Bryden and Stommel, 1984; Rohling et al., 2008). This can be accounted for, at least to first approximation, by considering a smaller value for coefficient c and thus for the water-flux ratio. Whether this is the dominant effect entailed by sea level variation will depend on the other characteristics of the basin. More realistic modelling and study of the transient response do require one accounts for the time rate-of-change of basin volume.

7. Conclusions

Basic principles, being conservation of water, salt and heat and a simple representation of strait flow, have been used to study the

behaviour of semi-enclosed seas. The main steps in the analysis and their results are the following:

(1) A dimensionless formulation sheds light on the interplay between basin area, basin depth, gateway efficiency and atmospheric forcing in controlling basin salinity and the time required for the basin to reach a steady state. Basin depth is shown to be a central factor in setting the time scale of the basin. Salinity responds to restriction in a very nonlinear way: even a gradual restriction will yield an event-like expression in the sedimentary record. The relationship between basin area and strait efficiency implies that, to have marginal basins reach gypsum saturation during the MSC, while the Mediterranean proper sits at normal salinity, would require unlikely small exchange fluxes.
(2) Representing the forcing as a generic periodic function of time, the analysis informs us how exactly basin salinity, its amplitude of variation and lag relative to the forcing, depends on basin and strait properties and varies with the period of forcing. Restriction or, more generally, a reduced water-flux ratio, introduces a lag in the response of basin salinity to variable net evaporation. This lag decreases for longer period of variation. Gypsum beds deposited during the MSC are most likely not centred on the peak of precession-paced aridity.
(3) Consideration of also the heat balance of the basin allows us to understand the relation between restriction and the mean air-sea heat flux and clarifies under which conditions heat flux and temperature play a role, in addition to net evaporation and salinity. Basins at least as restricted as the present Mediterranean Sea are shown to be intrinsically related to small annual-mean and basin-averaged air-sea heat flux. While in general the effect of heat/temperature appears less important than that of salinity, under certain conditions, heat flux and net evaporation together determine the sense of exchange at the sea strait.

Declaration of Competing Interest

The authors declare that they have no known competing financial interests or personal relationships that could have appeared to influence the work reported in this paper.

Acknowledgements

In developing the ideas presented in this paper I benefitted from discussions with many colleagues, in particular in the context of the MEDSALT, MEDGATE and SALTGIANT initiatives. Of these, Paco Sierro deserves special mention. Pieter Dirksen, Ronja Ebner and Alba de la Vara read earlier versions of parts of the manuscript. Xiangzhou Song assisted with questions on the Mediterranean heat budget. The editor Alessandra Negri, reviewer Gianluca Marino and an anonymous reviewer are thanked for their important role in shaping the final paper.

References

Ashkenazy, Y., Stone, P.H., Malanotte-Rizzoli, P., 2012. Box modeling of the Eastern Mediterranean sea. Phys. A Stat. Mech. Appl. 391, 1519–1531. https://doi.org/10.1016/j.physa.2011.08.026.
Astraldi, M., Balopoulos, S., Candela, J., Font, J., Gacic, M., Gasparini, G.P., Manca, B., Theocharis, A., Tintoré, J., 1999. The role of straits and channels in understanding the characteristics of Mediterranean circulation. Prog. Oceanogr. 44, 65–108. https://doi.org/10.1016/s0079-6611(99)00021-x.
Ben-Sasson, M., Brenner, S., Paldor, N., 2009. Estimating air–sea heat fluxes in semienclosed basins: the case of the Gulf of Elat (Aqaba). J. Phys. Oceanogr. 39 (1), 185–202. https://doi.org/10.1175/2008JPO3858.1.
Biton, E., Gildor, H., 2011. The general circulation of the Gulf of Aqaba (Gulf of Eilat) revisited: the interplay between the exchange flow through the Straits of Tiran and surface fluxes. J. Geophys. Res. 116 (C8), 104–115. https://doi.org/10.1029/2010JC006860.
Biton, E., Gildor, H., 2014. Energy budget of a small convectively driven marginal sea: the Gulf of Eilat/Aqaba (northern Red Sea). J. Phys. Oceanogr. 44, 1954–1972. https://doi.org/10.1175/JPO-D-13-0220.s1.
Bryden, H.L., Kinder, T.H., 1991. Steady two-layer exchange through the Strait of Gibraltar. Deep Sea Res. Part A Oceanogr. Res. Pap. 38, S445–S463. https://doi.org/10.1016/s0198-0149(12)80020-3.
Bryden, H., Stommel, H., 1984. Limiting processes that determine basic features of the circulation in the Mediterranean Sea. Oceanol. Acta 7 (3), 289–296.
Bryden, H., Candela, J., Kinder, T., 1994. Exchange through the Strait of Gibraltar. Prog. Oceanogr. 33, 201–428.
Buchanan, J.Y., 1877. On the distribution of salt in the ocean, as indicated by the specific gravity of its waters. J. R. Geogr. Soc. Lond. 47, 72–86. https://doi.org/10.2307/1798739.
Cessi, P., Pinardi, N., Lyubartsev, V., 2014. Energetics of Semienclosed Basins with Two-Layer Flows at the Strait. J. Phys. Oceanogr. 44 (3), 967–979. https://doi.org/10.1175/JPO-D-13-0129.1.
Criado-Aldeanueva, F., Soto-Navarro, F.J., Garcìa-Lafuente, J., 2012. Seasonal and interannual variability of surface heat and freshwater fluxes in the Mediterranean Sea: budgets and exchange through the Strait of Gibraltar. Int. J. Climatol. 32 (2), 286–302. https://doi.org/10.1002/joc.2268.
De Lange, G.J., Krijgsman, W., 2010. Messinian salinity crisis: a novel unifying shallow gypsum/deep dolomite formation mechanism. Mar. Geol. 275 (1–4), 273–277. https://doi.org/10.1016/j.margeo.2010.05.003.
Dirksen, J.P., Meijer, P., 2020. The mechanism of sapropel formation in the Mediterranean Sea: insight from long-duration box model experiments. Clim. Past 16, 933–952. https://doi.org/10.5194/cp-16-933-2020.
Drakopoulos, P.G., Lascaratos, A., 1999. Modelling the Mediterranean Sea: climatological forcing. J. Mar. Syst. 20, 133–157.
Falina, A., Sarafanov, A., Özsoy, E., Utku Turunçoğlu, U., 2017. Observed basin-wide propagation of Mediterranean water in the Black Sea. J. Geophys. Res. Oceans 122 (4), 3141–3151. https://doi.org/10.1002/2017JC012729.
García-Lafuente, J., Sammartino, S., Huertas, I.E., Flecha, S., Sánchez-Leal, R.F., Naranjo, C., Nadal, I., Bellanco, M.J., 2021. Hotter and weaker mediterranean outflow as a response to basin-wide alterations. Front. Mar. Sci. 8 https://doi.org/10.3389/fmars.2021.613444.
Garrett, C., 1996. The role of the Strait of Gibraltar in the evolution of Mediterranean water, properties and circulation. In: Bulletin de l'Institut Océanographique, Monaco, 17, pp. 1–19.
Garrett, C., Outerbridge, R., Thompson, K., 1993. Interannual variability in Mediterranean heat and buoyancy fluxes. J. Clim. 6 (5), 900–910. https://doi.org/10.1175/1520-0442(1993)006<0900:IVIMHA>2.0.CO;2.
Hilgen, F.J., Lourens, L.J., van Dam, J.A., 2012. The Neogene period. In: Gradstein, F., Ogg, J., Schmitz, M., Ogg, G. (Eds.), The Geological Time Scale 2012. Elsevier, Amsterdam, pp. 923–978.
Incarbona, A., Sprovieri, M., Lirer, F., Sprovieri, R., 2011. Surface and deep water conditions in the Sicily channel (central Mediterranean) at the time of sapropel S5 deposition. Palaeogeography Palaeoclimatology Palaeoecology 306, 243–248. https://doi.org/10.1016/j.palaeo.2011.04.030.
Johns, W.E., Yao, F., Olson, D.B., Josey, S.A., Grist, J.P., Smeed, D.A., 2003. Observations of seasonal exchange through the Straits of Hormuz and the inferred heat and freshwater budgets of the Persian Gulf. J. Geophys. Res. Oceans 108 (C12). https://doi.org/10.1029/2003JC001881.
Johnson, H.L., Cessi, P., Marshall, D.P., Schloesser, F., Spall, M.A., 2019. Recent contributions of theory to our understanding of the Atlantic meridional overturning circulation. J. Geophys. Res. Oceans 124 (8), 5376–5399. https://doi.org/10.1029/2019JC015330.
Jordà, G., Von Schuckmann, K., Josey, S.A., Caniaux, G., García-Lafuente, J., Sammartino, S., et al., 2017. The Mediterranean Sea heat and mass budgets: estimates, uncertainties and perspectives. Prog. Oceanogr. 156, 174–208. https://doi.org/10.1016/j.pocean.2017.07.001.
Knudsen, M., 1900. Ein hydrographischer lehrsatz. Ann. Hydrogr. Marit. Meteorol. 28 (7), 316–320.
Lugli, S., Manzi, V., Roveri, M., Schreiber, B., 2010. The Primary Lower Gypsum in the Mediterranean: a new facies interpretation for the first stage of the Messinian salinity crisis. Palaeogeogr. Palaeoclimatol. Palaeoecol. 297 (1), 83–99. https://doi.org/10.1016/j.palaeo.2010.07.017.
Macdonald, A.M., Candela, J., Bryden, H.L., 1994. An estimate of the net heat transport through the strait of Gibraltar. Coast. Estuar. Stud. 46, 13–32.
Maggiore, A., Zavatarelli, M., Angelucci, G., Pinardi, N., 1998. Surface heat and water fluxes in the Adriatic Sea: seasonal and interannual variability. Phys. Chem. Earth 23 (5), 561–567.
Manzi, V., Gennari, R., Lugli, S., Roveri, M., Scafetta, N., Schreiber, B.C., 2012. High-Frequency Cyclicity In the Mediterranean Messinian Evaporites: Evidence For Solar-Lunar Climate Forcing. Journal of Sedimentary Research 82, 991–1005. https://doi.org/10.2110/jsr.2012.81.
Manzi, V., Gennari, R., Hilgen, F., Krijgsman, W., Lugli, S., Roveri, M., Sierro, F.J., 2013. Age refinement of the Messinian salinity crisis onset in the Mediterranean. Terra Nova 25 (4), 315–322. https://doi.org/10.1111/ter.12038.
Marino, G., Rohling, E.J., Rijpstra, W.I.C., Sangiorgi, F., Schouten, S., Damsté, J.S.S., 2007. Aegean Sea as driver of hydrographic and ecological changes in the eastern Mediterranean. Geology 35, 674–675. https://doi.org/10.1130/g23831a.1.
Matthiesen, S., Haines, K., 2003. A hydraulic box model study of the Mediterranean response to postglacial sea-level rise. Paleoceanography 18 (4), 1–12. https://doi.org/10.1029/2003PA000880.
MEDAR Group, 2002. Medatlas 2002: Mediterranean and Black Sea Database of Temperature, Salinity and Biochemical Parameters; Climatological Atlas. IFREMER, Brest, France.

Meijer, P.T., 2006. A box model of the blocked-outflow scenario for the Messinian Salinity Crisis. Earth Planet. Sci. Lett. 248, 471–479. https://doi.org/10.1016/j.epsl.2006.06.013.

Meijer, P.T., 2012. Hydraulic theory of sea straits applied to the onset of the Messinian Salinity Crisis. Mar. Geol. 326-328 (C), 131–139. https://doi.org/10.1016/j.margeo.2012.09.001.

Meijer, P.T., Krijgsman, W., 2005. A quantitative analysis of the desiccation and re-filling of the Mediterranean during the Messinian Salinity Crisis. Earth Planet. Sci. Lett. 240, 510–520. https://doi.org/10.1016/j.epsl.2005.09.029.

Modestou, S., Simon, D., Gutjahr, M., Marzocchi, A., Kouwenhoven, T.J., Ellam, R.M., Flecker, R., 2017. Precessional variability of 87Sr/ 86Sr in the late Miocene Sorbas Basin: an interdisciplinary study of drivers of interbasin exchange. Paleoceanography 64 (1–2), 22–55. https://doi.org/10.1002/2016PA003061.

Natalicchio, M., Pierre, F.D., Birgel, D., Brumsack, H., Carnevale, G., Gennari, R., Gier, S., Lozar, F., Pellegrino, L., Sabino, M., Schnetger, B., Peckmann, J., 2019. Paleoenvironmental change in a precession-paced succession across the onset of the Messinian salinity crisis; Insight from element geochemistry and molecular fossils. Palaeogeography Palaeoclimatology Palaeoecology 518, 45–61. https://doi.org/10.1016/j.palaeo.2019.01.009.

Nielsen, J.N., 1912. Hydrography of the Mediterranean and adjacent waters. In: Schmidt, J. (Ed.), Report on the Danish Oceanographical Expeditions 1908–1910 to the Mediterranean and Adjacent Seas. Høst & søn, Copenhagen, pp. 77–191.

Özsoy, E., Ünlüata, Ü., 1997. Oceanography of the Black Sea: a review of some recent results. Earth-Sci. Rev. 42 (4), 231–272. https://doi.org/10.1016/s0012-8252(97)81859-4.

Pinardi, N., Zavatarelli, M., Adani, M., Coppini, G., Fratianni, C., Oddo, P., et al., 2015. Mediterranean Sea large-scale low-frequency ocean variability and water mass formation rates from 1987 to 2007: a retrospective analysis. Prog. Oceanogr. 132 (C), 318–332. https://doi.org/10.1016/j.pocean.2013.11.003.

Pinardi, N., Cessi, P., Borile, F., Wolfe, C.L.P., 2019. The Mediterranean sea overturning circulation. J. Phys. Oceanogr. 49, 1699–1721. https://doi.org/10.1175/jpo-d-18-0254.1.

Pratt, L.J., Whitehead, J.A., 2008. Nonlinear topographic effects in the ocean and atmosphere. Atmos. Ocean. Sci. Libr. 36. Springer, 589 pp.

Rogerson, M., Rohling, E.J., Bigg, G.R., Ramirez, J., 2012. Paleoceanography of the Atlantic-Mediterranean exchange: overview and first quantitative assessment of climatic forcing. Rev. Geophys. 50 (2) https://doi.org/10.1029/2011RG000376.

Rohling, E., Schiebel, R., Siddall, M., 2008. Controls on Messinian Lower Evaporite cycles in the Mediterranean. Earth Planet. Sci. Lett. 275 (1–2), 165–171.

Rohling, E.J., Foster, G.L., Grant, K.M., Marino, G., Roberts, A.P., Tamisiea, M.E., Williams, F., 2014. Sea-level and deep-sea-temperaturevariability over the past 5.3 million years. Nature 1–15. https://doi.org/10.1038/nature13230.

Roveri, M., Lugli, S., Manzi, V., Schreiber, B., 2008. The Messinian Sicilian stratigraphy revisited: new insights for the Messinian salinity crisis. Terra Nova 20 (6), 483–488.

Schroeder, K., Garcìa-Lafuente, J., Josey, S.A., Artale, V., Buongiorno, Nardelli B., Carrillo, A., Gacic, M., Gasparini, G.P., Marine, Herrmann, Lionello, P., Ludwig, W., Millot, C., Ozsoy, E., Pisacane, G., Sánchez-Garrido, J.C., Sannino, G., Santoleri, R., Somot, S., Struglia, M., Stanev, E., Taupier-Letage, I., Tsimplis, M.N., Vargas-Yanez, M., Zervakis, V., Zodiatis, G., 2012. Circulation of the Mediterranean sea and its variability. In: Lionello, P. (Ed.), The Climate of the Mediterranean Region: From the Past to the Future. Elsevier, Londres, pp. 187–256.

Sierro, F.J., Hodell, D.A., Andersen, N., Azibeiro, L.A., Jiménez-Espejo, F.J., Bahr, A., Flores, J.A., Ausin, B., Rogerson, M., Luz, R.L., Lebreiro, S.M., Hernández-Molina, F. J., 2020. Mediterranean overflow over the last 250 kyr: freshwater forcing from the tropics to the ice sheets. Paleoceanogr. Paleoclimatol. 35, 131–157. https://doi.org/10.1029/2020pa003931.

Simon, D., Meijer, P., 2015. Dimensions of the Atlantic-Mediterranean connection that caused the Messinian Salinity Crisis. Mar. Geol. 364 (C), 53–63. https://doi.org/10.1016/j.margeo.2015.02.004.

Smeed, D.A., 2004. Exchange through the Bab el Mandab. Deep-Sea Res. Part II Trop. Stud. Oceanogr. 51 (4–5), 455–474. https://doi.org/10.1016/j.dsr2.2003.11.002.

Sofianos, S., Johns, W.E., 2017. The summer circulation in the Gulf of Suez and its influence in the Red Sea thermohaline circulation. J. Phys. Oceanogr. 47 (8), 2047–2053. https://doi.org/10.1175/JPO-D-16-0282.1.

Sofianos, S.S., Johns, W.E., Murray, S.P., 2002. Heat and freshwater budgets in the Red Sea from direct observations at Bab el Mandeb. Deep-Sea Res. Part II Trop. Stud. Oceanogr. 49 (7), 1323–1340.

Song, X., Yu, L., 2017. Air-sea heat flux climatologies in the Mediterranean Sea: surface energy balance and its consistency with ocean heat storage. J. Geophys. Res. Oceans 122 (5), 4068–4087. https://doi.org/10.1002/2016JC012254.

Topper, R.P.M., Meijer, P.T., 2013. A modeling perspective on spatial and temporal variations in Messinian evaporite deposits. Mar. Geol. 336, 44–60. https://doi.org/10.1016/j.margeo.2012.11.009.

Topper, R.P.M., Meijer, P.T., 2015. The precessional phase lag of Messinian gypsum deposition in Mediterranean marginal basins. Palaeogeogr. Palaeoclimatol. Palaeoecol. 417 (C), 6–16. https://doi.org/10.1016/j.palaeo.2014.10.025.

Tsimplis, M.N., Zervakis, V., Josey, S.A., Peneva, E.L., Struglia, M.V., Stanev, E.V., et al., 2006. Chapter 4 Changes in the oceanography of the Mediterranean Sea and their link to climate variability. In: Developments in Earth and Environmental Sciences, 4, pp. 227–282. https://doi.org/10.1016/s1571-9197(06)80007-8.

Tziperman, E., Speer, K., 1994. A study of water mass transformation in the Mediterranean Sea: analysis of climatological data and a simple three-box model. Dyn. Atmos. Oceans 21 (2), 53–82.

Verri, G., Pinardi, N., Oddo, P., Ciliberti, S.A., Coppini, G., 2018. River runoff influences on the Central Mediterranean overturning circulation. Clim. Dyn. 50 (5–6), 1675–1703. https://doi.org/10.1007/s00382-017-3715-9.

Wessel, P., Smith, W.H.F., Scharroo, R., Luis, J., Wobbe, F., 2013. Generic mapping tools: improved version released. EOS Trans. AGU 94 (45), 409–410. https://doi.org/10.1002/2013EO450001.

Whitehead, J., 1998. Topographic control of oceanic flows in deep passages and straits. Rev. Geophys. 36 (3), 423–440.

Yari, S., Kovacevic, V., Cardin, V., Gačić, M., Bryden, H.L., 2012. Direct estimate of water, heat, and salt transport through the Strait of Otranto. J. Geophys. Res. 117 (C9) https://doi.org/10.1029/2012JC007936 n/a–n/a.

Zhang, Z., Ramstein, G., Schuster, M., Li, C., Contoux, C., Yan, Q., 2014. Aridification of the Sahara desert caused by Tethys Sea shrinkage during the Late Miocene. Nature 513 (7518), 401–404. https://doi.org/10.1038/nature13705.